Characterization and Optimization of Intelligent Reflective Surfaces in mm-Wave Band including the Reflection Produced by the Building Structure

Á. F. Vaquero[1,2], E. Martinez-de-Rioja[3], M. Arrebola[1*], and J. A. Encinar[4]

[1]Department of Electrical Engineering, Universidad de Oviedo, Spain
[2]Instituto de Telecomunicações, Universidade de Lisboa, Portugal
[3]Dep. of Signal Theory and Communications and Telematic Systems and Computing, Universidad Rey Juan Carlos, Spain
[4]Information Processing and Telecommunications Center, Universidad Politécnica de Madrid, Spain
[*]Corresponding author: arrebola@uniovi.es

Abstract

This work presents the design and optimization of a passive Intelligent Reflective Surface (IRS) based on a reflectarray technology to improve the coverage in a mm-Wave 5G scenario. A preliminary design is performed to achieve a wide beam in azimuth and elevation. The IRS is placed on a building façade and its effect is electromagnetically characterized for different materials. The design is then improved by optimizing the IRS considering the wall where it is placed.

1. Introduction

In the recent years, Smart Electromagnetic Skins (SMEs) have been proposed to overcome the issues related to signal propagation because of the physical barriers in the deployment of novel wireless networks in mm-Wave scenarios [1]. Namely, Intelligent Reflective Surfaces (IRS) are used to enhance 5G FR2 coverage avoiding the installation of multiple base stations (BS). An IRS is a planar surface made up of phase-shifting elements that reflect the impinging signal radiated from the BS into a desired direction (specular or another direction). The reflected field could be either a beam pointing or even a shaping beam. Active or passive phase-shifting elements can be used in the panel, mainly depending on the reconfiguration required by the coverage. Moreover, IRS has been also proposed to introduce beam tilting in a pointing direction to overcome the so-called blind zones, which are defined as an area of poor or even null coverage [2]. When the IRS is based on passive elements it is called SME.

IRS have been proposed for both urban and indoor scenarios [3], [4]. In both cases, the walls are usually the most suitable placements for installing the reflective surface. In a general scenario, the BS is far away from the IRS, therefore only a small fraction of the radiated power provided by the BS is captured by the IRS. This small fraction must be properly managed to enhance the coverage. Owing to the BS is far away, the surroundings of the IRS are also strongly illuminated so that the spillover on the building façade cannot be negligible.

The reflection produced by the surrounding wall should be characterized and considered for an accurate modeling of the coverage provided to the devices of the users as Figure 1 shows. If this effect is not taken into account the coverage could be not the desired one, having a significant distortion in the coverage link. Thus, the coverage synthesis and the IRS design should be carried out considering this major effect. Moreover, the limits in the achievable coverage should be also studied, to avoid unfeasible goals in the design and optimizations process.

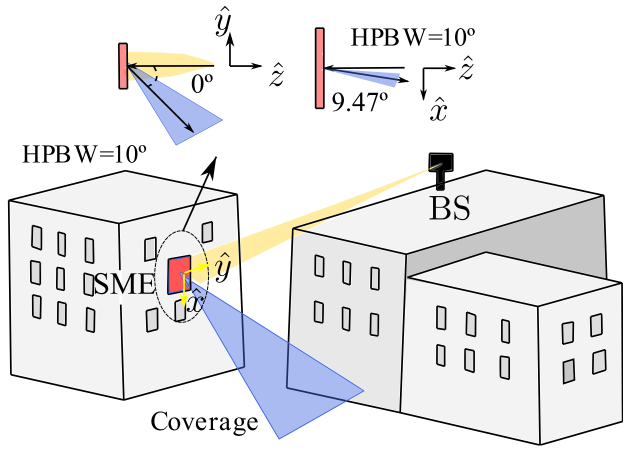

Figure 1. Sketch of a 5G scenario using an IRS to enhance the coverage. The BS illuminates the IRS that generates a coverage to overcome a blind area.

2. Smart Electromagnetic Skin Design

2.1. Scenario and Smart Electromagnetic Skin Optics

The Intelligent Reflective Surface is based on a passive panel, so that it is called a Smart Electromagnetic Skin. In this case, the SME is designed for an outdoor scenario. The aim is placing the panel in a building face to enhance the coverage provided by a base station. A similar case as the one of Figure 1 is proposed for this design. The BS is placed at 30 m in the **z**-direction and at height of 5 m in the **x**-direction. The panel is used to enhance the coverage in the specular direction since there is a blind area with poor coverage due to physical barriers (wall, building, etc.).

The panel does not only reflect the incident wave but also to produce a broad beam in both azimuth and elevation. The specifications in terms of beam pointing and half-power beamwidth (HPBW) are shown in Figure 1. Mainly, the panel operates at 27.7 GHz widening the beam 10º in both azimuth and elevation, resulting in a square coverage. Since the

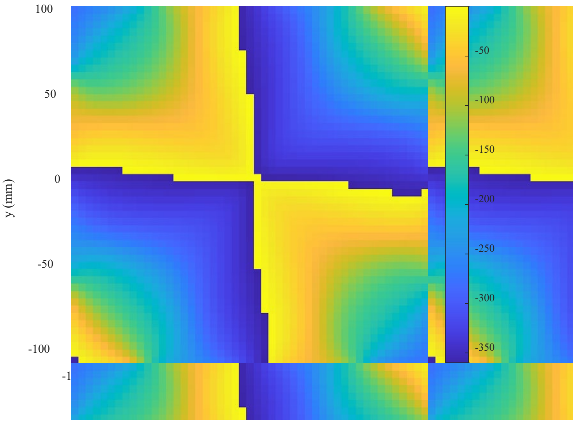

Figure 2. Phase-shift distribution of the elements of the SME obtained after the POS.

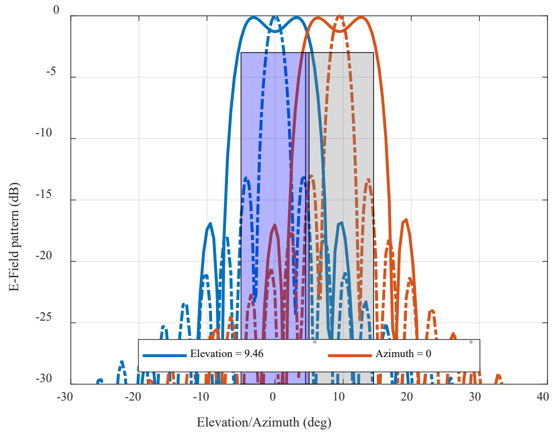

Figure 3. Normalized E-field pattern computed in the main cuts of the coverage for the V-polarization before (dotted line) and after (solid line) the synthesis at 27.7 GHz.

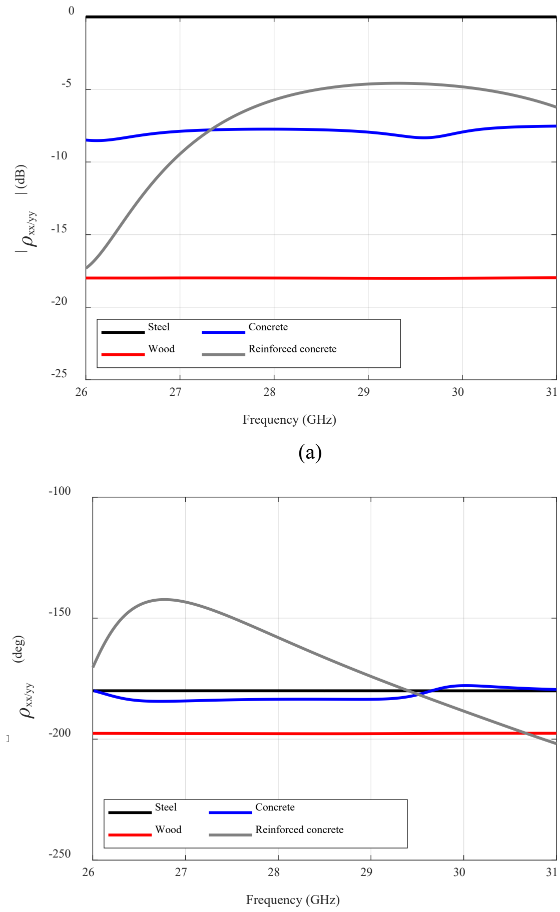

(b)

Figure 4. Reflection coefficient of the analyzed materials at several frequencies considering normal incidence (a) amplitude (dB) (b) phase (deg).

incident wave is reflected in the specular, the outgoing angles are 9.47º in elevation and 0º in azimuth.

The panel is dual-linearly polarized considering the horizontal polarization (H) defined according to the **y**-axis, while the vertical polarization (V) is defined in the **x**-axis.

To achieve the desired specifications the reflective SME is comprised of 50 x 50 elements of periodicity 4.29 x 4.29 mm^2.

2.2. Design procedure

As a first attempt, the SME is designed to radiate a pencil beam in the desired direction following (1) to compute the phase-shift of the elements:

$$\phi(x_l, y_l) = k_0(|\boldsymbol{d}_l| - (x_l \cos\varphi_0 + y_l \sin\varphi_0) \sin\theta_0) \qquad (1)$$

where k_0 is the wavenumber in vacuum, (θ_0, φ_0) are the pointing direction of the pencil beam, in this case 9.47° and 0°, respectively. $\boldsymbol{d}_l$ is the distance from the feed $(x_{BS}, y_{BS}, z_{BS}) = (-5, 0, 30)$ m and the lth element, and (x_l, y_l) are the coordinates of the lth element referred to the center of the SME.

This solution provides a narrow beam whose half-power beamwidth is around 2º. Therefore, this configuration does not provide a successful solution, requiring widening the beam in both azimuth and elevation to fulfill the specifications

To obtain the broadened beam, the phase-shift distribution of the SME computed using (1) is synthesized using a Phase-Only Synthesis (POS) technique. The aim is to synthesize the phase of the reflection coefficients of the elements to finally find a proper distribution that radiates the desired pattern. To do so, the classical technique based on the Intersection Approach [5],[6] is used to reach the broadened beam with a ripple lower than 3 dB. Note that, during this process, the elements are modeled as ideal elements and the output of the synthesis is the phase-shift distribution that produces the desired co-polar pattern.

The synthesis procedure is based on a multi-stage process to improve the convergence of the algorithm. This procedure is commonly used when dealing with a large number of elements (in this case 2500), since the elements are the number of unknowns to be solved in the synthesis for each polarization. Figure 2 shows the phase-shift distribution that should introduce each element in both linear polarizations. Then, Figure 3 shows the main cuts of the co-polar pattern of the starting point and the synthesized phase-shift distribution for the V-polarization. Since the synthesis is based on ideal

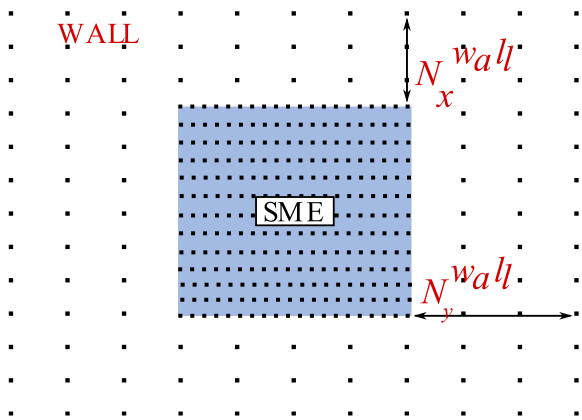

Figure 5. Sketch of the discretization of the whole array (SME plus wall).

elements, the results for the H-polarization are nearly the same.

In the light of these results, the beam is properly widened in both directions, reaching a square coverage of 10º by 10º. Furthermore, the ripple is quite low, having an almost flat-top beam in both azimuth and elevation. Therefore, it satisfies the requirements of ripple.

3. Electromagnetic response of the wall

The SME is designed for an outdoor scenario, so that the panel will be installed in a building façade. Considering that the BS is far away and provides a beam with wide HPBW (in this case about 12°), the incident field will have a strong illumination also in the surrenders of the SME, producing a high spillover. Comparing the electrical size of the SME and the façade, the SME will only capture a low fraction of the radiated power, while the spillover will be high. Therefore, the reflection produced by the wall should be analyzed to evaluate its influence on the coverage.

To do so, the wall should be firstly characterized. We have evaluated different materials to obtain their electromagnetic response. In this case, the materials analyzed are concrete ($\epsilon_r = 5.45, \tan\delta = 0.0021$), reinforced concrete ($\epsilon_r = 12.8, \tan\delta = 0.0021$), wood $\epsilon_r = 1.54, \tan\delta = 0.033$) and steel ($\sigma = 7.69 * 10^6$ S/m). The electromagnetic characterization of the materials is extracted from the libraries of CST Microwave Studio [7].

Those materials are analyzed in CST Microwave Studio to obtain the reflection coefficient. The analysis is carried out considering a block of 120-mm thick made up of the corresponding material under analysis. The block is analyzed considering local periodicity environment, ant it is illuminated by a uniformed-linearly-polarized plane wave propagating in the **z**-direction. The four materials are analyzed within a band of 4 GHz, from 26 to 30 GHz.

Note that the analysis is carried out using a uniformed-linearly-polarized plane wave, since the distance between the BS and the SME is large enough to consider the real incident field as a plane wave. Furthermore, the angles of incidence on both SME and surrounding area will be low enough to only consider normal incidence.

Figure 4 shows the amplitude and phase of the reflection coefficients (ρ_{xx} and ρ_{yy}). As might be expected, the greater

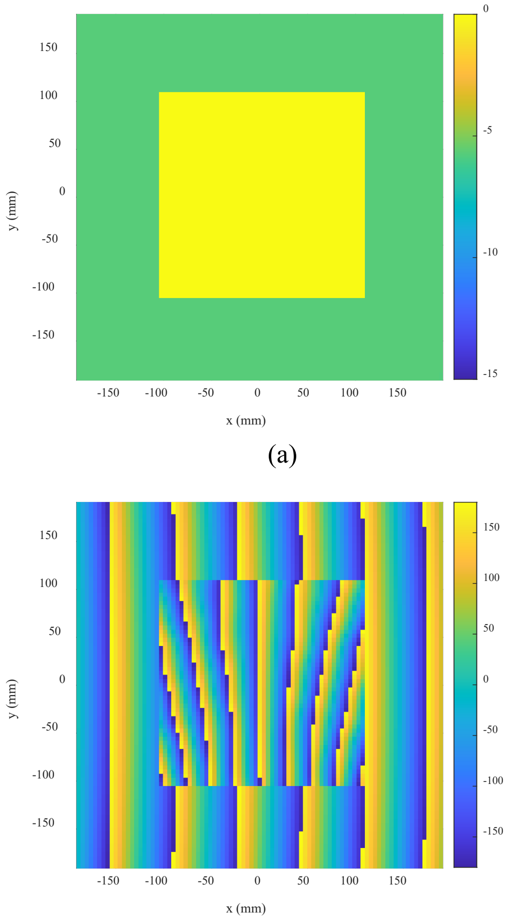

(a)

(b)

Figure 6. (a) Normalized amplitude (dB) and (b) phase (deg) of the reflected field onto the SME surface and the wall at 27.7 GHz.

the presence of steel (or other metals), the greater the reflection produced. The response of steel can be approximated by the reflection produced by a Perfect Electrical Conductor (PEC), while the wood might be considered as transparent since it barely reflects the wave (at least within this bandwidth).

4. Effect of the wall on the coverage

4.1. Computation of the wall in the radiation pattern

Once the electromagnetic characterization of the wall is obtained, its influence on the coverage can be obtained. We are going to assume that the panel is centered in a wall. Now, the wall and the SME will be assumed as a whole, having a larger SME. To do so, the wall is also divided into unit cells, considering the same periodicity of the SME. The new SME (wall plus SME) is comprised of $N_x \times N_y$ elements that are extended $N_x^{wall} \times N_y^{wall}$ elements in **x-** and **y**-direction, respectively. Therefore, the total size of the new SME is $(N_x + 2N_x^{wall}) \times (N_y \times 2N_y^{wall})$. Figure 5 shows further details on how the elements are distributed.

The radiated field of the whole SME is computed by means of contributions [8]. The aperture is divided into subdomains

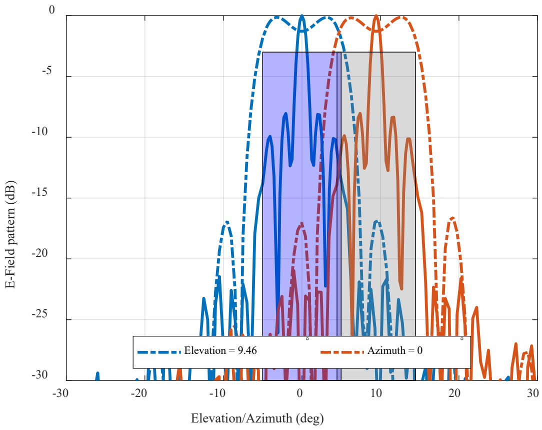

Figure 7. Normalized E-field pattern computed in the main cuts of the coverage for the V-polarization (dotted line) after the synthesis only considering the SME (solid line) after the synthesis considering the wall at 27.7 GHz.

that are associated to a single element of the SME. Then, the radiated field can be expressed as

$$\boldsymbol{E}_R(\boldsymbol{r}) = \sum_{n=1}^{N_x}\sum_{m=1}^{N_y} \boldsymbol{E}_{SME}^{mn}(\boldsymbol{r}) + \sum_{p=1}^{N_x^{wall}}\sum_{l=1}^{N_y^{wall}} \boldsymbol{E}_{wall}^{pl}(\boldsymbol{r}) \tag{2}$$

where $\boldsymbol{E}_{SME}$ is the contribution of the nm-th elements of the original SME at the observation point $\boldsymbol{r}$, and $\boldsymbol{E}_{wall}$ is the contribution of the pl-th element of the wall.

Both contributions $\boldsymbol{E}_{SME}$ and $\boldsymbol{E}_{wall}$ can be computed using the classical theory of planar apertures, since the SME and wall are considered as a planar radiating aperture. Those contributions require knowing the tangential field onto the aperture surface. The tangential field is obtained from the incident field and the reflection matrix $\overline{\boldsymbol{R}}$**.** In this case, we must consider two reflection matrices, one for the SME elements (4), and one for the wall elements (5). In the case of the SME the elements are modeled as ideal phase shifters, so that they are lossless and only introduce a delay in the incident wave. Moreover, only the co-polar pattern is computed. This approximation is valid since the losses of the elements are quite low in reflective surfaces. However, in the wall the elements are fully characterized considering the reflection coefficients as a complex number. It is important to consider the loss of the material, otherwise there will be no difference between steel or wood, just on the introduced delay. Furthermore, the elements of the wall introduce the same phase delay and loss, since all of them are under normal incidence.

$$\overline{\boldsymbol{R}}_{SME} = \begin{pmatrix} \rho_{xx}^{mn} & \rho_{xy}^{mn} \\ \rho_{yx}^{mn} & \rho_{yy}^{mn} \end{pmatrix} = \begin{pmatrix} e^{j\phi_{xx}^{mn}} & 0 \\ 0 & e^{j\phi_{yy}^{mn}} \end{pmatrix} \tag{4}$$

$$\overline{\boldsymbol{R}}_{wall} = \begin{pmatrix} \rho_{xx}^{pl} & \rho_{xy}^{pl} \\ \rho_{yx}^{pl} & \rho_{yy}^{pl} \end{pmatrix} = \begin{pmatrix} |\rho_{xx}|e^{j\phi_{xx}} & 0 \\ 0 & |\rho_{yy}|e^{j\phi_{yy}} \end{pmatrix} \tag{5}$$

4.2. Distortion on the coverage produced by the wall

To compute the effect of the wall we assume that the wall has an area of 0.480×0.480 m^2, being the SME area 0.215×0.215 m^2 (it is centered in the wall as Figure 5 shows). Therefore, the wall extends the array in 20 elements from each edge of the SME, so that the new array is 90×90 elements. Figure 6 shows the reflected field considering the whole array, for the case of concrete. It should be noted that the illumination taper at the edge of the SME is less than 1 dB. The amplitude of the reflected field along the SME surface barely changes, having a uniform reflection, while the amplitude in the wall is attenuated due to the losses of the material (reinforced concrete). The phase clearly changes in the area wherein the SME is placed, while the wall only introduces a delay in the incident field (being the same delay for each cell).

Applying (2) to compute the radiated field, we obtain the radiation pattern shown in Figure 7. This radiation pattern is clearly distorted regarding Figure 3, mainly due to the strong specular reflection produced by the wall. Although the field level increases, the shaped beam is shattered.

5. Conclusions

In this work, a SME is proposed to enhance the coverage of a 5G network in mm-Wave band. A synthesis technique is used to obtain a phase-shift distribution of the SME elements that generates a widened beam. Specifically, a flat-top beam of $10° \times 10°$ in azimuth and elevation, with the aim of covering a blind coverage area. The antenna is designed and the effect on the radiation pattern is evaluated once it is placed on a façade. For this purpose, a simple model based on the Principle of Superposition is introduced, which allows taking into account the field reflected by the wall (spillover). It is observed that the shaped beam is shattered, mainly because the contribution of the wall is much higher than the one of the SME. For this reason, the design of SME or, in general IRS, must consider the environment where the antenna is located. Therefore, the optimization or synthesis processes used in the antenna design must be extended to include these new effects. Additionally, the used of higher directivity beams to illuminate the IRS (or SME), as well as the use of larger aperture should be also analyzed to overcome those effects.

Acknowledgements

This work was supported by MICIN/AEI/10.13039/501100011033 within projects PID2020-114172RB-C21-2; by the Spanish Ministry of Universities and European Union (NextGenerationEU fund) under project MU-21-UP2021-03071895621J; by Gobierno del Principado de Asturias under project AYUD/2021/51706; and by de Comunidad de Madrid within the Multiannual Agreement Framework with Universidad Rey Juan Carlos, Line of Action 1, Young Researchers R&D Project INCREASE-5G (Ref. F858).

References

[1] G. Oliveri, P. Rocca, M. Salucci, and A. Massa, Holographic Smart EM Skins for Advanced Beam Power Shaping in Next Generation Wireless Enviroments, *IEEE Journal on Multiscale and Multiphysics*

Computational Techniques, vol. 6, pp. 171-182, Oct. 2022.

[2] K. Zheng, D. Wang, Y. Han, X. Zhao, and D. Wang, Performance and measurements analysis of a commercial 5G millimeter-wave network, *IEEE Access*, vol. 8, pp. 163996-164011, 2020.

[3] E. Martinez-de-Rioja, Á. F. Vaquero, M. Arrebola, E. Carrasco, J. A. Encinar and M. Achour, Passive Dual-Polarized Shaped-Beam Reflectarrays to Improve Coverage in Millimeter-Wave 5G Networks, *2021 15th European Conference on Antennas and Propagation (EuCAP)*, Dusseldorf, Germany, pp. 1-5, 2021.

[4] E. Martinez-de-Rioja *et al.*, Enhancement of 5G Millimeter-Wave Coverage in Indoor Scenarios by Passive Shaped-Beam Reflectarray Panels, *2022 16th European Conference on Antennas and Propagation (EuCAP)*, Madrid, Spain, pp. 1-5, 2022.

[5] O. M. Bucci, G. D'Elia, and G. Romito, Power synthesis of conformal arrays by a generalized projection method, *IEE Proc. Microw. Antennas Propag.*, vol. 142, no. 6, pp. 467-471, Dec. 1995.

[6] D. R. Prado *et al.*, Efficient Crosspolar Optimization of shaped-beam dual-polarized reflectarrays using full-wave analysis for the antenna element characterization, *IEEE Transactions on Antennas and Propagation*, vol. 65, no. 2, pp. 623-635, Feb. 2017.

[7] Systèmes, Dassault, CST microwave studio [Computer program], Available at : http://www.cst.com [Accessed : 14 October 2022].

[8] Á. F. Vaquero, M. Arrebola, M. R. Pino, R. Florencia, and J. A. Encinar, Demonstration of a reflectarray with near-field amplitude and phase constraints as Compact Antenna Test Range probe for 5G new radio devices, *IEEE Transactions on Antennas and Propagation*, vol. 69, no. 5, pp. 2715-2726, May 2021.